Why is Dawsonite Absent in CO$_2$ Charged Reservoirs?

H. Hellevang, J. Declercq and P. Aagaard

Department of Geosciences, University of Oslo, Pb. 1047, Blindern, Oslo - Norway
e-mail: helghe@geo.uio.no - julien.declercq@geo.uio.no - per.aagaard@geo.uio.no

Résumé — Pourquoi la dawsonite est-elle absente des réservoirs chargés en CO$_2$? — La possibilité pour la dawsonite – un hydroxy-carbonate de sodium et d'aluminium (NaAl(OH)$_2$CO$_3$) – de précipiter dans les aquifères salins dès lors que l'on y injecte du CO$_2$ a été suggérée dans maintes simulations menées sur différentes compositions (minéraux et solution aqueuse) et dans des conditions de pression et de température variées. Pourtant, sur le strict plan de la stabilité thermodynamique, la dawsonite paraît moins communément répandue que l'on pourrait s'y attendre dans les analogues naturels de stockages de CO$_2$.

On a cartographié la stabilité thermodynamique de la dawsonite par rapport à des phases minérales comme l'albite, la kaolinite et l'analcime, entre 37 et 200 °C, puis on a simulé numériquement des évolutions minérales en système fermé à l'aide d'un nouveau formalisme cinétique pour la précipitation, formalisme qui inclut (1) un terme de nucléation, basé sur la théorie classique de la nucléation, et (2) un terme de croissance, dérivant de la théorie BCF de la croissance. Utilisant cette équation de vitesse, on a réalisé une étude de sensibilité pour examiner comment la croissance de la dawsonite varie avec la composition minérale, la température, la pression partielle de CO$_2$, la vitesse de nucléation – et les variations de cette dernière avec la température et l'affinité chimique –, et enfin la constante de vitesse adoptée pour la loi de précipitation de la dawsonite. Lorsqu'on empêche la dawsonite de précipiter, le rapport de sur-saturation ne dépasse jamais 3 ou 4 pour des solutions de type eau de mer. La propension accrue à précipiter si la pression partielle de CO$_2$ augmente est contrebalancée par l'effet d'acidification de la solution. Diminuer jusqu'à 5 ordres de grandeur la vitesse de précipitation n'a qu'un effet limité sur le démarrage d'une croissance significative, et au bout de 1 000 ans de simulation la quantité de dawsonite formée est de 37 % ce qu'elle est dans le régime de précipitation maximale. Réduire le taux de nucléation a le même effet de retarder la croissance du minéral. Au bout du compte, sur la base de considérations thermodynamiques et au vu des simulations présentées, on suggère que le potentiel de croissance de la dawsonite est restreint à une fenêtre de températures médianes. À basse température, la stabilité relativement grande de la dawsonite vis-à-vis des minéraux en compétition est contrecarrée par la forte diminution des vitesses de nucléation et de croissance, ce qui reflète une puissante barrière énergétique.

*Abstract — **Why is Dawsonite Absent in CO$_2$ Charged Reservoirs?** — Growth of the sodium-aluminium-hydroxy carbonate dawsonite (NaAl(OH)$_2$CO$_3$) after charging saline aquifers with CO$_2$ has been assumed in a plethora of numerical simulations at different mineralogies, aqueous solutions, pressures and temperatures. It appears however that dawsonite is less abundant than expected in natural CO$_2$ storage analogues if we take into account the thermodynamic stability alone.*

We have mapped the thermodynamic stability of dawsonite relative to mineral phases like albite, kaolinite and analcime from 37° to 200°C and performed closed-system batch kinetic simulations using a new kinetic expression including a nucleation term based on classical nucleation theory, and a growth term that was based on BCF growth theory. Using this rate equation, we have performed a sensitivity study on dawsonite growth on mineralogy, temperature, CO$_2$ pressure, nucleation rate and its

dependencies on temperature and affinity, and on the dawsonite precipitation rate coefficient. Simulations with dawsonite growth disabled showed that the maximum oversaturation reached for dawsonite for seawater-like solutions never exceeded 3-4 times oversaturation. The positive effect on dawsonite growth of increasing the CO_2 pressure was mostly neutralized by higher acidity. Decreasing the precipitation rate coefficient by 5 orders of magnitude had a limited effect on the onset of significant growth, but the amount of dawsonite formed at the end of the 1 000 years simulated time was only 37% below the high-rate case. Reducing the nucleation rates had similar effects leading to postponed dawsonite growth. Finally, based on thermodynamic considerations and numerical simulations, we suggest that the potential of dawsonite growth is limited to a medium-temperature window framed by a high thermodynamic stability relative to competing mineral phases at low temperatures, but with rapidly diminishing nucleation and growth rates at lower temperatures constrained by energy barriers.

INTRODUCTION

The fourth assessment report of the Intergovernmental Panel on Climate Change (IPCC) showed that it is likely that increasing rates of CO_2 emissions to the atmosphere will contribute to a global temperature rise of our planet (IPCC, 2007). One way to reduce emission rates is to capture CO_2 from large anthropogenic point sources and inject the carbon into underground geological aquifers (IPCC, 2005; Gale, 2004; Holloway, 1997). As the CO_2 is injected it dissolves into the aqueous solution and reacts to form carbonic acid. The perturbation in acidity leads to dissolution of the reservoir minerals and formation of new stable phases. Of importance for safe long-term storage of CO_2 is the formation of carbonate minerals. The reservoirs potential of forming these carbonates is partly given by the amount of divalent metal cations present in the reservoir, which may vary from low in quartz rich sands like the Utsira Sand (*e.g.*, Chadwick *et al.*, 2004), to medium and high for glauconitic and "Gulf-Coast" type reservoirs respectively (*e.g.*, Xu *et al.*, 2004). However, a mineral that may add significantly to this potential is dawsonite ($NaAl(OH)_2CO_3$) which has been suggested to play a significant role as a CO_2 storage host in saline alkaline aqueous solutions with a moderate to high CO_2 pressure (Johnson *et al.*, 2004; Worden, 2006).

Dawsonite is reported to be abundant in natural reservoirs that are currently at a high CO_2 pressure, or that have previously experienced an influx of CO_2 (Baker *et al.*, 1995; Gao *et al.*, 2009; Golab *et al.*, 2006, 2007; Moore *et al.*, 2005; Smith and Milton, 1966; Worden, 2006). By its elevated thermodynamic stability at highly alkaline conditions (*e.g.*, Hellevang *et al.*, 2005), dawsonite is commonly found associated with $NaHCO_3$-elevated brines reacting with alumino-containing minerals. One example of extensive dawsonite formation from such highly alkaline solutions is the Green River Formation of Colorado (Smith and Milton, 1966). Dawsonite is found together with analcime ($NaAlSi_2O_6·H_2O$) and carbonates such as nahcolite ($NaHCO_3$), both indicating highly alkaline conditions. Dawsonite may also form at acidic conditions such as in the Triassic Lam Formation in the Shabwa Basin, Yemen, where it is found at concentrations of up to 8% of the sediment (Worden, 2006). Detailed petrological investigations suggests that at temperatures from 85 to 100ºC, feldspars have reacted with CO_2 and high-NaCl brines formed dawsonite together with quartz. Albite in perthitic feldspars have been replaced by dawsonite whereas the potassium part remained unaltered (Worden, 2006). Similar reactions have been observed for the Hailaer Basin in Northeastern China where feldspars in arkoses and lithic arkoses have been replaced by dawsonite and microquartz by interaction with CO_2 and waters at temperatures between 85 and 105ºC (Gao *et al.*, 2009). Dawsonite was in this case interpreted as a late-stage diagenetic mineral following illite and kaolinite formation.

Although dawsonite is abundant locally as in the Green River and Lam Formations, it is not always present after long-term interactions between sediments and aqueous solutions at high CO_2 pressures. For example, Gaus *et al.* (2004) examined mineral reactions following long-term interactions with CO_2 for the Montmiral, Southeast Basin, France, at present-day 100ºC and 360 bar, and Messokampos, Florina Basin, Greece, at maximum 10 bar and 43ºC (Gaus *et al.*, 2004). The Montmiral reservoir contains high-NaCl brines with salinities of about 3 times seawater, and K-feldspar that could act as an aluminium source for dawsonite growth. Analyses of the Montmiral waters suggests that dawsonite is close to saturation or slightly supersaturated (Pauwels *et al.*, 2007). No dawsonite has however been observed (Gaus *et al.*, 2004; Pauwels *et al.*, 2007). The Messokampos reservoir has lower salinity than seawater, but abundant Na-feldspar and the high pH of 8.7 should in this case favour dawsonite growth. The fairly low NaCl content of the waters and the low temperatures and CO_2 partial pressures are probably the reason for the lack of dawsonite growth in this case. Another example of natural CO_2-charged reservoir that appears to lack dawsonite growth is found in the shallow Bravo Dome natural CO_2 field in New Mexico (Pearce *et al.*, 1996). Detailed petrographic studies shows extensive corrosion of plagioclase from CO_2-charged acidified waters and formation of authigenic minerals. No dawsonite was observed.

At present no information is available on the nucleation rate of dawsonite and information regarding the growth rate is very limited. Numerous reports have shown how gibbsite or kaolinite reacted in sodium carbonate or bicarbonate solutions at high pH easily transform into dawsonite at temperatures from 120 to 200°C (*e.g.*, Bénézeth *et al.*, 2007; Zhang *et al.*, 2004; Duan *et al.*, 2005; US patent #4.221.771). At present the report by Duan *et al.* (2005) provides the most extensive data on conversion rates of aluminosilicates and aluminohydroxides into dawsonite at temperatures down to 75°C. The experiments by Duan *et al.* (2005) converted 1% kaolinite to dawsonite at 75°C during 40 days of reactions and 1% of gibbsite at 94°C during 24 hours. A crude estimate based on information in the Duan *et al.* (2005) abstract (Na/Al molar ratio 8, molar concentration $NaHCO_3$ = 4.81) gives a 75°C kaolinite to dawsonite conversion rate of 2.34×10^{-11} moles/s and 94°C gibbsite to dawsonite conversion rate of 5.66×10^{-10} moles/s. Based on the conversion rates, we estimated the reaction rate coefficient of dawsonite assuming $r = kS(\Omega - 1)$, an average reactive surface area of 0.1 m², and 2 000 times dawsonite supersaturation estimated by the PHREEQC speciation code (Parkhurst and Appelo, 1999) using the llnl.dat database and assuming $NaHCO_3$ and aluminium concentrations given by nahcolite and gibbsite saturations respectively, we get reaction rate coefficients of 1.17×10^{-13} and 2.83×10^{-12} moles/m²s respectively from kaolinite and gibbsite. These rates are indeed orders of magnitude slower than the corresponding dawsonite dissolution rate coefficients reported by Hellevang *et al.* (2005, 2010), but is in the same range as estimated kaolinite (*e.g.*, Carroll-Webb and Walther, 1988; Bauer and Berger, 1998) and gibbsite (Nagy and Lasaga, 1992) dissolution rates at these conditions. At this point we can thus only assume that the precipitation rates of dawsonite at high supersaturations are faster than the aluminium source dissolution rates and we can not exclude the fast dawsonite precipitation rates as predicted from the dissolution rate experiments. As dawsonite dissolution rates have just recently been reported (Hellevang *et al.*, 2005, 2010), calculations up to present on the potential of carbonate storage have employed reaction rates of dawsonite based on proxy minerals like siderite (Gherardi *et al.*, 2007; Xu *et al.*, 2007; Zhang *et al.*, 2009), calcite (White *et al.*, 2005), or rates that are intermediate between calcite and magnesite or dolomite (André *et al.*, 2007; Cantucci *et al.*, 2009; Gaus *et al.*, 2005; Johnson *et al.*, 2004; Knauss *et al.*, 2005).

Numerical simulations, both equilibrium path calculations and estimates of reactions constrained by kinetic expressions suggest that dawsonite form in a large variety of geological environments spanning from low to high temperatures and from different mineral assemblages (*e.g.*, Harrison *et al.*, 1995; Johnson *et al.*, 2004; Knauss *et al.*, 2005; Xu *et al.*, 2004, 2007; Zerai *et al.*, 2006). Dawsonite growth rates are commonly modeled using knowledge on the dissolution rates and mechanisms through expressions derived from the Transitions State Theory (TST) and the law of detailed balancing (see Lasaga, 1984; Aagaard and Helgeson, 1982). According to TST, derivatives of the rates with respect to parameters like temperature and affinity are assumed to vary continuously over the equilibrium state as long as the same mechanism is assumed responsible for the rates. This does not make physical sense as the mechanisms responsible for the dissolution and precipitation rates respectively, *e.g.* breakup or formation of bonds, do vary over the equilibrium state. This is clear if we compare dissolution and precipitation rates for common carbonates. One example is magnesite where the dissolution rate coefficient at 100°C (Pokrovsky *et al.*, 2009) is 4 to 5 orders larger than the precipitation rate coefficient as reported by Saldi *et al.* (2009), and the differences in activation energies, reflecting different reaction mechanisms, are similarly large. Moreover, precipitation rate experiments on minerals like magnesite (Saldi *et al.*, 2009), calcite (Shiraki and Brantley, 1995), dolomite (Arvidson and Mackenzie, 1997, 1999) and quartz (Ganor *et al.*, 2005) suggests that the reaction order of precipitation with respect to affinity of these minerals may be better explained by growth models such as the BCF (Burton Cabrera and Frank) crystal growth theory (Burton *et al.*, 1951) than the TST, and that no single model can explain the reaction rates over the whole affinity range (Shiraki and Brantley, 1995). An additional challenge in using the simplified TST-derived equations for estimating dawsonite formation results from lack of a term including nucleation preceding growth.

The aim of this work is to improve our ability to predict dawsonite formation using equilibrium thermodynamics and kinetic simulations. The estimates are based on closed-systems were the potential for dawsonite growth is limited to the local supply of sodium and aluminium from the aqueous solution and the reacting mineral assemblage. To understand how physical conditions relevant to CO_2 storage affects the relative stability of dawsonite, the thermodynamic stability of dawsonite relative to some common aluminosilicates in the $Na_2O-Al_2O_3-SiO_2-CO_2-H_2O$ system is mapped as a function of temperature and CO_2 pressure. The possibility of dawsonite formation in the $K_2O-Na_2O-Al_2O_3-SiO_2-CO_2-H_2O$ system is discussed briefly. The kinetic simulations were divided into two parts, the first employing the commonly used TST-derived rate equations on various mineralogies and physical conditions, and the second using a modified rate equation. The latter simulations were done because the traditional TST-derived rate laws fail in capturing differences in dissolution and precipitation rate mechanisms, and do not include any nucleation barrier or nucleation rate. We propose a rate equation divided into an undersaturated and an oversaturated part each with a set of rate parameters. We used published rate parameters for the dissolution part, whereas rate parameters which are unknown for the precipitation part were varied. The precipitation rate equation was divided into a growth part corresponding to close-to-equilibrium BCF-growth, and a nucleation part simplified from classical theory on heterogeneous nucleation rates.

1 STABILITY OF DAWSONITE

The stability of dawsonite can be understood by mapping the thermodynamic stability of the mineral relative to other mineral phases competing for aluminium. The natural choice of system to consider is the Na_2O-Al_2O_3-SiO_2-CO_2-H_2O system which includes competing phases such as albite, kaolinite and analcime at given CO_2 pressures. The system includes the phases involved in the dawsonite precipitation experiments by Duan *et al.* (2005) and knowledge on the system may thus be used to understand their experiments. Because potassium phases such as K-feldspar, muscovites and illites are common phases in sedimentary basins, their possible role as aluminium source for dawsonite growth is discussed as well.

Thermodynamic data for species included in the activity diagrams except for dawsonite were calculated by the SUPCRT92 program (Johnson *et al.*, 1992) using the dprons96.dat database. The Gibbs free energy of dawsonite was calculated from the dissociation reaction given in the PHREEQC LLNL database which is based on thermodynamic values from Ferrante *et al.* (1976), and by using the free energies of its components estimated from the SUPCRT92 program. Solubility of CO_2 was calculated using the PHREEQC code with pre-calculated fugacity coefficients according to the Soave-Redlich-Kwong (Soave, 1972) equation of state (SRK EOS), and corrected for at temperatures above 100°C by a poynting correction term.

1.1 The Na_2O-Al_2O_3-SiO_2-CO_2-H_2O System

Dawsonite stability in saline aquifers at varying CO_2 pressures can be understood by comparing relative stabilities of aluminosilicates and sodium carbonates in aqueous activity diagrams. Phases that are commonly associated with dawsonite growth at elevated CO_2 pressures are albite and kaolinite. The dawsonite precipitation experiments by Duan *et al.* (2005) produced analcime but no dawsonite upon reacting phases such as albite and pyrophyllite at 150 and 200°C. The thermodynamic stability of analcime relative to dawsonite, kaolinite and albite is thus also added to the activity diagrams.
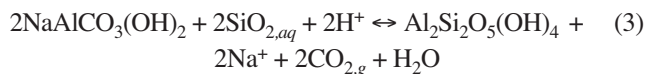
If we assume that aluminium is conserved in mineral phases, the dawsonite stability relative to albite can be written as:

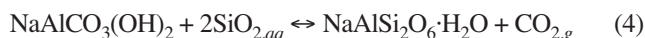$$NaAlCO_3(OH)_2 + 3SiO_{2,aq} \leftrightarrow NaAlSi_3O_8 + CO_{2,g} + H_2O \quad (1)$$
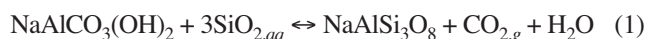
where subscripts *aq* and *g* denotes water and gas phases respectively. The silica activity at the univariant divide between dawsonite and albite is then given by:

$$\log a_{SiO_2,aq} = -\frac{1}{3}\log K_{(1)} + \frac{1}{3}\log f_{CO_2} \quad (2)$$

where *a* and *f* denote activity and fugacity, and $K_{(1)}$ is the equilibrium constant for reaction (1). This means that dawsonite is unstable relative to albite at any silica activities higher than the value given by Equation (2). Similar relations can be drawn for the stability of dawsonite relative to kaolinite and analcime:

$$2NaAlCO_3(OH)_2 + 2SiO_{2,aq} + 2H^+ \leftrightarrow Al_2Si_2O_5(OH)_4 + \quad (3)$$
$$2Na^+ + 2CO_{2,g} + H_2O$$

and

$$NaAlCO_3(OH)_2 + 2SiO_{2,aq} \leftrightarrow NaAlSi_2O_6 \cdot H_2O + CO_{2,g} \quad (4)$$

respectively where the silica activities for the univariant lines are given by:

$$\log a_{SiO_2,aq} = \log\left(\frac{a_{Na^+}}{a_{H^+}}\right) - 0.5\log K_{(3)} + \log f_{CO_2} \quad (5)$$

and

$$\log a_{SiO_2,aq} = -\frac{1}{2}\log K_{(4)} + \frac{1}{2}\log f_{CO_2} \quad (6)$$

where $K_{(3)}$ and $K_{(4)}$ denote equilibrium constants for reactions (3) and (4) respectively. It is evident from these relations that the thermodynamic stability of dawsonite relative to albite, kaolinite and analcime is dependent on pH, and the aqueous activities of Na^+, CO_2, and SiO_2.

The stability of dawsonite as a function of $\log a_{SiO_2,aq}$ and the log activity ratio of Na^+ over H^+ at 37°, 75° and 100°C at CO_2 partial pressures of 100, 200 and 300 respectively is shown in Figure 1. The stability is plotted relative to albite, gibbsite and kaolinite and with quartz, amorphous silica, and nahcolite saturations superimposed. The dawsonite stability region is shown as the gray shaded area. The figure shows that at 37°C, silica activities at quartz and amorphous silica saturations are well within the stability region of dawsonite. At 75 and 100°C silica activities at quartz or amorphous silica saturation approach the univariant divide between albite and dawsonite. The red lines and filled circles in the diagrams show likely solution compositions for dawsonite growth. At 37°C solutions are likely to precipitate amorphous silica or chalcedony fixing the silica activity at higher values. The upper limit for the Na^+ over H^+ activity ratio is likely given by nahcolite. At temperatures of 75°C or higher, quartz precipitation rates likely becomes fast enough to force aqueous silica activities close to quartz saturation (*e.g.*, Bjørlykke and Egeberg, 1993). If we use the distance from the aqueous chemical composition within the dawsonite stability field, *e.g.* the red line in Figure 1, to the albite-dawsonite univariant line as a proxy for the thermodynamic driving force of the albite-dawsonite transformation, then increasing temperature lowers this thermodynamic driving force.
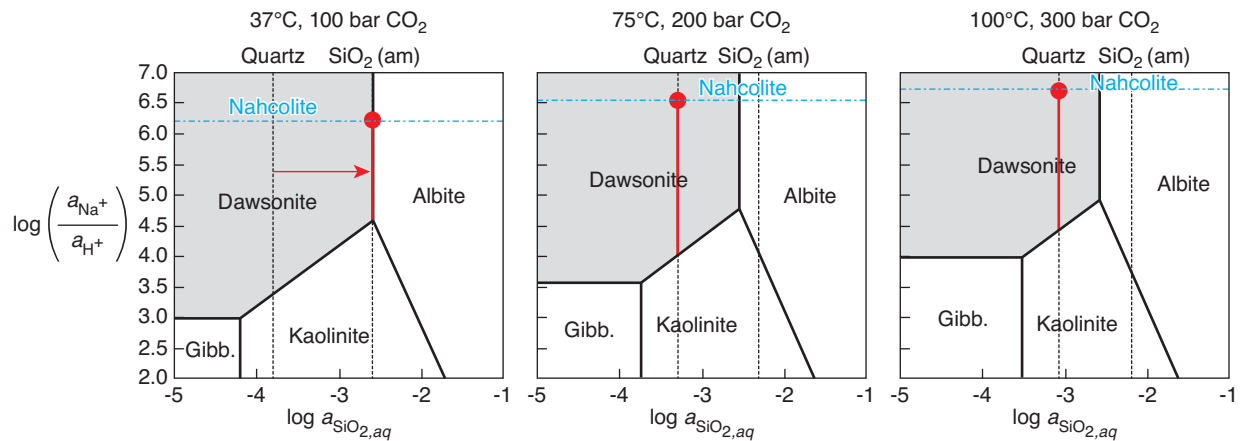
Figure 1

Aqueous activity diagrams which show the stability of dawsonite, gibbsite and albite at 37, 75 and 100°C and at 100, 200 and 300 bar CO_2 respectively. The saturated values of quartz, amorphous silica and nahcolite is superimposed on the diagrams. Red lines denote likely silica activities given by amorphous silica at low temperature (37°C) and quartz at 75° and 100°C.
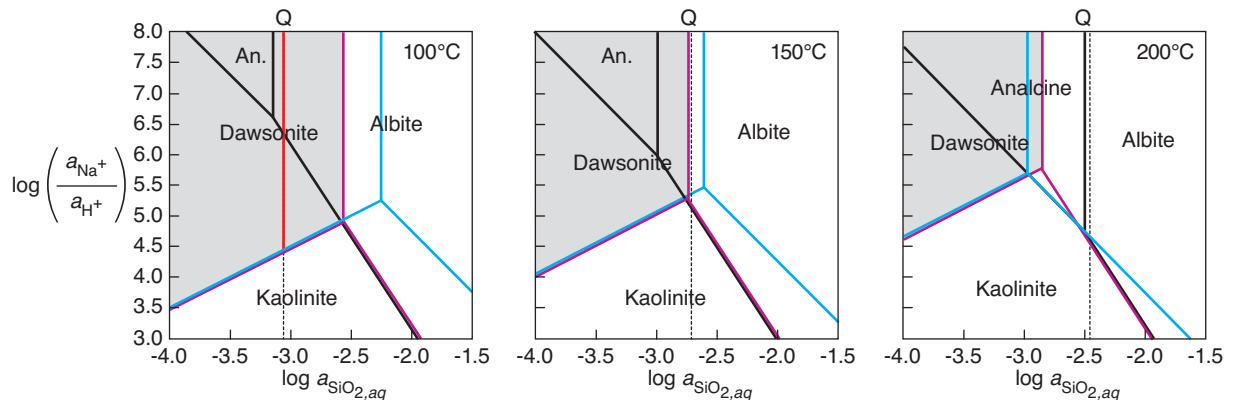

Figure 2

Aqueous activity diagrams which show the stability of dawsonite relative to albite, kaolinite and analcime at 100-200°C and 300 bar CO_2. Red mineral divide lines denote the three-mineral assemblage albite-dawsonite-kaolinite, blue lines the three-mineral assemblage analcime-dawsonite-kaolinite, and black lines denote the three-mineral assemblage analcime-albite-kaolinite. Shaded gray area illustrate the stability of dawsonite relative to albite and kaolinite. The solubility of quartz (Q) is illustrated as a dotted line. The red line within the dawsonite stability field at 100°C is where the quartz saturation is within the dawsonite stability field.

The stability of dawsonite relative to aluminosilicates at 100, 150 and 200°C at a fixed CO_2 pressure of 300 bar is shown in Figure 2. The figure illustrates how aqueous silica may inhibit dawsonite growth at high temperatures typical for hydrothermal synthesis experiments. The relative stability of analcime increases with temperature and is included together with albite and kaolinite. The dawsonite stability relative to albite and kaolinite, shown as red lines in Figure 2, is shown to decrease with increasing temperatures. At 150°C or higher temperatures the superimposed quartz saturation line is in the albite stability field suggesting that dawsonite will not form from albite at these conditions. At 200°C analcime has reached high enough stability relative to albite and kaolinite, seen as black lines, to make an albite-kaolinite assemblage metastable at quartz-undersaturation conditions. At lower CO_2 pressures, the dawsonite stability would diminish further and lead to even higher relative stabilities of albite, kaolinite and analcime. The elevated analcime stability at high temperature and the dependence of dawsonite stability on CO_2 pressure may explain the experiments by Duan *et al.* (2005) forming analcime instead of dawsonite at high temperatures but at CO_2 pressures lower than the 300 bar given for the stabilities in Figure 2. At any CO_2 fugacity and temperature, elevated silica stabilize the aluminosilicates relative to dawsonite.
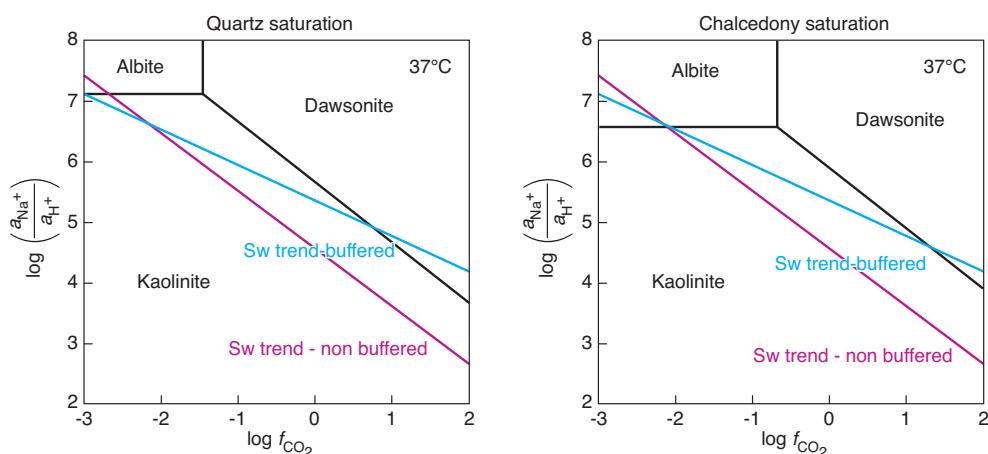
Figure 3

The thermodynamic stability of dawsonite with respect to aqueous solutions at 37°C as a function of CO_2 fugacity *versus* the sodium over hydrogen activity ratio. Superimposed are lines that correspond to seawater values buffered and not buffered by calcium carbonate equilibrium.

By fixing the silica activity, the dawsonite stability can be visualized at varying CO_2 fugacities. This is shown in Figure 3 that shows the stability of dawsonite as a function of the aqueous sodium to hydrogen activity ratio and the fugacity of CO_2 at quartz and chalcedony saturation at 37°C. Superimposed on the diagram are two aqueous solutions representing unbuffered seawater after Nordstrom *et al.* (1979), and the same seawater buffered by calcite equilibrium. It is clear from the figure that at a given silica activity elevated CO_2 pressures and high sodium concentrations stabilize dawsonite relative to kaolinite. However, the superimposed seawater solutions show that, because of the pH drop caused by increasing CO_2 pressures, dawsonite is not stable unless calcite or other carbonate buffers are present and buffer the pH drop. Moreover, the CO_2 pressure required to stabilize dawsonite relative to the aluminosilicates is dependent on the silica activity. At quartz saturation dawsonite is stable down to fugacities below 10, whereas at chalcedony saturation fugacities of 20-30 are required to stabilize dawsonite. At higher silica activities even higher CO_2 pressures are required.

1.2 Muscovite or K-feldspar as Al-sources for Dawsonite Growth?

Because K-feldspar and muscovite-like illites are common minerals in sedimentary basins the possibility for dawsonite growth from these phases and the relation to diagenetic processes is briefly discussed. The stability of K-feldspar is closely related to diagenetic processes like illitization and albitization. At low temperatures (80-110°C), illite forms mainly by alteration of smectites (*e.g.*, Eslinger and Pevear, 1988; Bjørlykke *et al.*, 1992). At higher temperatures illite may

form from the metastable K-feldspar-kaolinite mineral assemblage (Ehrenberg and Nadeau, 1989; Bjørlykke *et al.*, 1992):

$$KAlSi_3O_8 + Al_2Si_2O_5(OH)_4 \rightarrow$$
$$KAl_3Si_3O_{10}(OH)_2 + 2SiO_{2,aq} + H_2O \qquad (7)$$
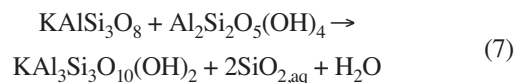
increasing the silica activity leading to quartz growth. For details on phase relationships in the K_2O-Al_2O_3-SiO_2-H_2O diagrams see Aja *et al.* (1991). In the absence of kaolinite, K-feldspar dissolution increases the potassium activity and places aqueous solutions along the stable K-feldspar-illite univariant stability curve preserving the K-feldspar. At low potassium activities, K-feldspar may be destabilized and form albite at temperatures above 65°C (Saigal *et al.*, 1988; Aagaard *et al.*, 1990). This process is again limited by the increasing aqueous potassium activity as the albitization proceeds. As will be shown for the kinetic simulations, a ideal reaction like (7) do not perfectly describe non-equilibrium systems constrained by the rates of the minerals reactions, and some aluminium may be supplied for dawsonite growth from the K-feldspar-kaolinite-muscovite mineral assemblage. Aagaard *et al.* (2009) showed that for a sedimentary reservoir like Utsira Sand at 37°C and 100 bar CO_2, the likely reaction in the K_2O-Al_2O_3-SiO_2-H_2O system after the CO_2 perturbation is the dissolution of muscovite and albite leading to K-feldspar and kaolinite formation.

1.3 Dawsonite Reaction Rates

The first data on the dissolution rate of dawsonite was reported by Hellevang *et al.* (2005). This report, based on natural dawsonite, suggested that the dissolution rate was close to

the magnesite reaction rate with a far-from-equilibrium dissolution rate of 1.58×10^{-9} mol/m²s at 80°C and apparently without any pH dependence at $3.5 < \text{pH} < 8.6$ (Hellevang *et al.*, 2005). More recent comprehensive experiments on synthetic dawsonite extended the knowledge on the reaction rates of dawsonite to lower pHs (Hellevang *et al.*, 2010). The new data suggests that the far-from-equilibrium dissolution rates at acidic to circumneutral conditions can be represented by one single rate expression taking into account a proton-promoted dissolution mechanism that dominates at strongly acidic conditions and a hydration-driven mechanism dominating at circum-neutral conditions (Hellevang *et al.*, 2010):

$$r_+ = S \left\{ 10^{3.43} a_{H^+} \exp\left(\frac{-44600}{RT}\right) + 10^{5.26} \exp\left(\frac{-80600}{RT}\right) \right\} \quad (8)$$

where S is reactive surface area, a is activity, R is the gas constant (J/K·mol) and T is absolute temperature. The apparent activation energy for the proton promoted dissolution was similar to what has been reported for magnesite (Pokrovsky *et al.*, 2009), whereas the apparent activation energy at circumneutral- to basic conditions was much higher (-80.6 kJ/mol).

As already shown in the introduction, some limited information on dawsonite precipitation rates is available from the work done by Duan *et al.* (2005) on dawsonite synthesis at high supersaturations. Calculations suggests that dawsonite precipitation rates at temperatures of 75 and 94ºC are equal to or faster than kaolinite and gibbsite dissolution rates. No information is however yet available on the precipitation rates at low (<75ºC) temperatures and at realistic supersaturations for CO₂ storage scenarios in sedimentary basins.

2 GEOCHEMICAL SIMULATIONS

2.1 Methods

As a first approach, mineral reaction kinetics were estimated according to an expression derived from transition state theory (Lasaga, 1981, 1984; Aagaard and Helgeson, 1982):

$$r = kS \prod_i a_i^{v_i} \exp\left(-\frac{Ea}{RT}\right) f(\Delta G) \quad (9)$$

where k is the reaction rate coefficient, S is reactive surface area, a and v are the activity and the reaction order of solutes

affecting the rates respectively, and the thermodynamic driving force function f is given by:

$$f(\Delta G) = 1 - \Omega \quad (10)$$

where $\Omega = \exp(\Delta G/RT)$ denotes the affinity of the reaction with respect to the aqueous solution, R is the gas constant and T is absolute temperature. The reactive surface area S was calculated by:

$$S = \beta M n \quad (11)$$

where β is the Brunauer-Emmet-Teller (BET) surface area (Brunauer *et al.*, 1938), M is the molar weight and n is the number of moles of the mineral, whereas the reactive surface area for precipitation was equal to 1% of the total sediment surface area. This number, representing a fraction of the total surface area, has no direct physical meaning but is in the range of what have been used in other numerical studies on mineral formation during CO₂ storage (*e.g.*, Gaus *et al.*, 2005; Johnson *et al.*, 2004). Expressions (9) and (10) with various expressions for the reactive surface area are the preferred choice for numerical simulations of CO₂ mineral storage (Gaus *et al.*, 2005; Ketzer *et al.*, 2009; Wigand *et al.*, 2008; Xu *et al.*, 2007; Zhang *et al.*, 2009).

One major limitation of expressions such as Equation (9) is that the mineral nucleation rate and a nucleation barrier is not included for the initial stage of mineral formation. This may lead to overestimation of carbonate growth during CO₂ storage as phases such as dawsonite or magnesite generally are not present in reservoirs prior to CO₂ injection. The rate of heterogeneous nucleation can be expressed as (Nielsen, 1964; Walton, 1967):

$$J = k_N \exp\left\{ -\beta N_A f(\theta) \left(\frac{v \sigma^{3/2}}{(RT)^{3/2} \ln \Omega} \right)^2 \right\} \quad (12)$$

where the pre-exponential factor k_N is the nucleation rate constant, β is a geometric shape factor, N_A is Avogadro's number, $f(\theta)$ is a correction factor for heterogenous nucleation, v is molar volume, and σ is surface tension. This means that no nuclei will form at infinite low supersaturations an that fewer and larger nuclei forms at low temperatures and low supersaturations (Walton, 1963; Nielsen, 1964). To examine how sensitive dawsonite formation is on nucleation, we defined a new set of equations combining Equations (9) and (12): (see *Eq. 13*)

$$r = \begin{cases} k_d S_d a_i^{v_d} \exp\left(-\dfrac{Ea_d}{RT}\right)\{1 - \Omega\} & \text{if} \quad \Omega \le 1 \\[4ex] -k_p S_p a_i^{v_p} \exp\left(-\dfrac{Ea_P}{RT}\right)\{\Omega - 1\}^2 - k_N \exp\left\{ -\Gamma\left(\dfrac{1}{(T)^{3/2} \ln \Omega}\right)^2 \right\} & \text{if} \quad \Omega > 1 \end{cases} \quad (13)$$

where k is the kinetic coefficient at a given temperature, subscripts d, p and N denote dissolution, precipitation and nucleation respectively, and Γ contains all parameters except T and Ω in the exponential term in Equation (12). The second-order dependence of growth on affinity is predicted from BCF-theory for screw-dislocation dominated growth (Burton *et al.*, 1951). Because k_p and Γ are not known for dawsonite, we varied these parameters and looked at the sensitivity on dawsonite formation. Although values were not known for Γ, it was chosen to vary from 10^9 to 10^{10} which resulted in reasonable values of nucleation rates at various supersaturations *(Fig. 4)*. The nucleation rate coefficient, k_N, was similarly unknown and chosen arbitrarily as 10^{-8} moles/s giving reasonable nucleation rates *(Fig. 4)*. The activation energy for precipitation Ea_p was set at the same value as for dissolution Ea_d *(Tab. 1)*. For the second set of simulations using Equation (13), the growth surface area for dawsonite was estimated by Equation (11), using the specific surface area for crushed dawsonite as reported for the dissolution rate experiments. This assumption likely lead to an underestimate of the specific surface area of the growing dawsonite because of the initial growth from small nuclei and crystals. The sensitivity on the potential of dawsonite growth on the reactive growth surface area is however provided through varying the growth rate coefficient k_p by 5 orders of magnitude, which has the same effect on the rate as varying the S_p by the same magnitude.

Table 1 lists parameters for Equation (9). Kinetic constants listed are reported kinetic constants from published reports divided on the Arrhenius term exp(–Ea/RT). Integration of

mineral reaction rates, CO_2 phase equilibria, and aqueous speciation were solved using the numerical code PHREEQC-2 (Parkhurst and Appelo, 1999) with the LLNL.DAT database based on the thermo.com.V8.R6.230 database prepared at the Lawrence Livermore National Laboratory. As the ideal gas law is used in PHREEQC-2 for gas phases, input partial pressures were corrected for by a fugacity coefficient and a poynting correction term to make CO_2 solubility calculations accurate. The input partial pressure was calculated by:

$$ f = P\phi_{SRK} \cdot \exp\left\{ -\frac{\bar{v}_{CO_2}}{RT}\left(P - P_{sat}\right) \right\} \qquad (14) $$

where ϕ is the fugacity coefficient of CO_2 calculated by the Soave-Redlich-Kwong (SRK) equation of state (Soave, 1972), P is pressure, T is temperature, R is the gas constant, $\bar{v}$ is the partial molar volume of CO_2, and subscript *sat* denotes saturation pressure.

2.2 Dawsonite Formation in Shallow Quartz-dominated Reservoirs

The potential of dawsonite formation in shallow quartz dominated reservoirs was simulated using data from the Utsira formation at the Sleipner CO_2 injection site. The temperature and pressure were set to 37°C and 100 bar respectively, corresponding to a CO_2 fugacity of 56.99 estimated by the SRK EOS (Soave, 1972). Reactions were calculated
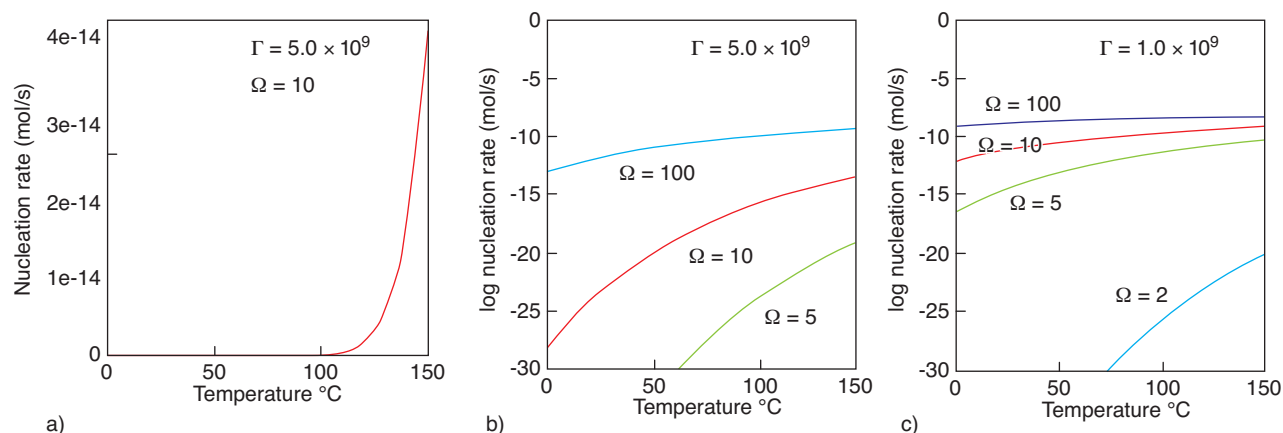

Figure 4

The nucleation rate calculated by the second term in the precipittion part of Equation (13) using a fixed k_N of 10^{-8} mols/s. Because no information is available about nucleation rates of dawsonite we varied the Γ parameter over a range giving reasonable nucleation rates over varying temperatures and supersaturations. a) Shows the temperature dependence of estimated nucleation rates at 10 times oversaturation ($\Omega = 10$), an $\Gamma = 5 \times 10^9$; b) and c) shows estimated nucleation rates as a function of affinities at $\Gamma = 5 \times 10^9$ and 1×10^9 respectively.

TABLE 1

Kinetic parameters used for calculating the mineral reaction rates

Minerals	k^a (mol/m²s)	E_a (J/mol)	S (m²/g)	References
Quartz	24	87 700	0.0225	Tester *et al.* (1994)
Chalcedony[b]	24	87 700	0.0225	Tester *et al.* (1994)
Albite	0.726	67 700	0.1	Blum and Stillings (1995)
K-feldspar	1.15×10^{-3}	51 700	0.11	Brantley (2008)
Dawsonite	1.82×10^{5}	80 600	9.8	Hellevang *et al.* (2010)
Kaolinite	4.42×10^{-8}	29 300	11.2	Carroll-Webb and Walther (1988)
Muscovite	4.83×10^{-4}	58 200	0.68	Oelkers *et al.* (2008)
Clinochlore-14A	0.3653	66 000	1.6	Brandt *et al.* (2003)
Montmorillonite	1.16×10^{-2}	66 000	44	Golubev *et al.* (2006)
Magnesite	2.02×10^{-3}	37 700	0.127	Pokrovsky *et al.* (2009)

[a] Kinetic constant k as used in Equation (9). The pH dependence (a_{H^+}) is taken from the cited reports.
[b] Chalcedony used the same kinetic parameters as for quartz, but with the affinity term based on thermodynamic data on chalcedony.

TABLE 2

Initial mineral fractions (mass%) and porosities for the two different sand types that corresponds to the Utsira Sand and a Gulf Coast type of sand

Minerals	Mass percent	
	"Utsira"[a] (37°C)	"Gulf Coast"[b] (75°C)
Quartz	75	58
K-feldspar	13	8.2
Calcite	3	1.93
Aragonite	3	0
Albite	3	19.8[c]
Muscovite	2.05[d]	1.0
Kaolinite	0.95[d]	2.02
Na-montmorillonite[e]	0	4
Clinochlore 14A[f]	0	4.55
Porosity	35%	30%

[a] Values after Chadwick *et al.* (2004).
[b] Values from Xu *et al.* (2007). 0.5 mass% hematite was not included.
[c] Used instead of oligoclase (Na₀.₈) as reported by Xu *et al.* (2007)
[d] Mica and others group comprises 3% of the Utsira Sand (Chadwick *et al.*, 2004). Divided into muscovite and kaolinite here based on the clay fraction of the utsira caprock (Chadwick *et al.*, 2004).
[e] Used as a proxy for the Na-smectite reported in Xu *et al.* (2007).
[f] Uses as a proxy of the chlorite reported in Xu *et al.* (2007).

assuming closed boundaries for the aqueous phase, but at a constant CO₂ pressure corresponding to exchange through the system boundaries with an infinite CO₂ reservoir. The mineralogy listed in Table 2 was chosen similar to the one reported by Chadwick *et al.* (2004). Formation water data *(Tab. 3)* was modified from Johnson *et al.* (2004) which in turn modified data reported from a sample taken at Oseberg. This water is similar in salinity and with a composition close to seawater. Two additional simulations using 1 and 2 molar NaCl solutions, referred to as medium- and high salinity cases *(Tab. 3)*, were done to see how the formation water NaCl content affects the saturation states of dawsonite. Dawsonite growth was disabled in these simulations as the motivation was to see the potential level of supersaturations at increasing salinities. In addition, as the stability diagrams suggests that buffering of the pH by calcite or other minerals is necessary to stabilize dawsonite *(Fig. 3)*, the potential of dawsonite formation was simulated including and excluding calcite buffering in the system.

Figure 5 shows the mass percentage of dawsonite, the dawsonite solubility index $SI = \log(\Omega)$, and the pH evolution after CO₂ injection over 1 000 years. The simulation including calcite at equilibrium starts precipitating dawsonite immediately after CO₂ injection, and the pH, buffered by the calcite dissolution, stay at a constant value at approximately 4.9. Because the reaction rate of dawsonite is fast compared to the dissolving aluminium source minerals such as albite, dawsonite forms at close to equilibrium. The overall rate of the silicate to dawsonite reaction is hence constrained by the dissolution of albite and K-feldspar that supply Al. Because both albite and K-feldspar are close to equilibrium ($SI \sim 0.01$), the overall transformation rate is slow. To quantify the

importance of each individual mineral to supply aluminium for the dawsonite growth, a simple mass balance was performed for the K-feldspar-kaolinite-muscovite system, and for the amount of dawsonite formed compared to the amount of albite dissolved *(Fig. 6)*. Figure 6a shows the temporal evolution of the moles of potassium and aluminium conserved in the K-feldspar-kaolinite-muscovite system. It is evident from this figure that some aluminium is supplied for dawsonite growth, with a maximum of 0.025 moles after approximately 550 years *(Fig. 6a)*. The system initially take up some aqueous potassium, before it is conserved and constant *(Fig. 6a)*. To illustrate that the released aluminium shown in Figure 6a correspond to the amount taken up in the dawsonite, we estimated the residual of the excess dawsonite growth compared to albite dissolved, and the aluminium lost from the K-feldspar-kaolinite-muscovite system *(Fig. 6b)*. We see that the residual fluctuates at low values around zero, proving that dawsonite grew from both K-feldspar and kaolinite in addition to the albite. We finally estimated the percentage of dawsonite that grew from albite *(Fig. 6c)*, and we see that the values drop to a minimum of 55% after 150 years, before it increases and approaches 85% after 1 000 years. An extrapolation to longer time-scales would suggest that aluminium is supplied back to the K-feldspar-kaolinite-muscovite system *(Fig. 6a, c)*, and that only albite would be the final source for the dawsonite.

For the case without calcite the other mineral reactions buffers the pH change up to pH > 4.5 after a few hundred
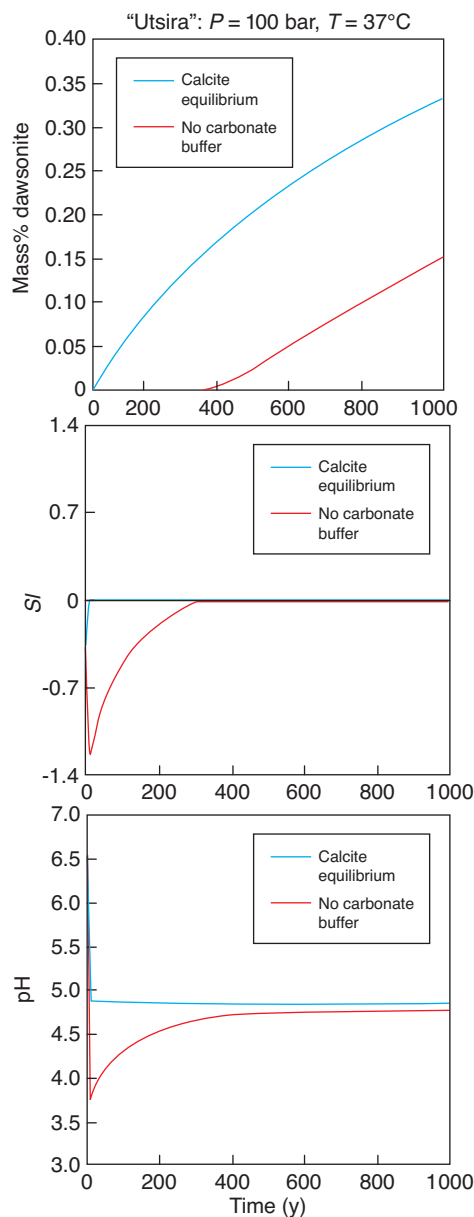
Figure 5

Mass percent dawsonite, the dawsonite solubility index $SI = \log(q/K)$, and pH as a function of time for the "Utsira" case that corresponds to 100 bar C_2 and a temperature of 37°C. Two different cases are showed, pH buffered and not buffered respectively by calcite equilibrium.
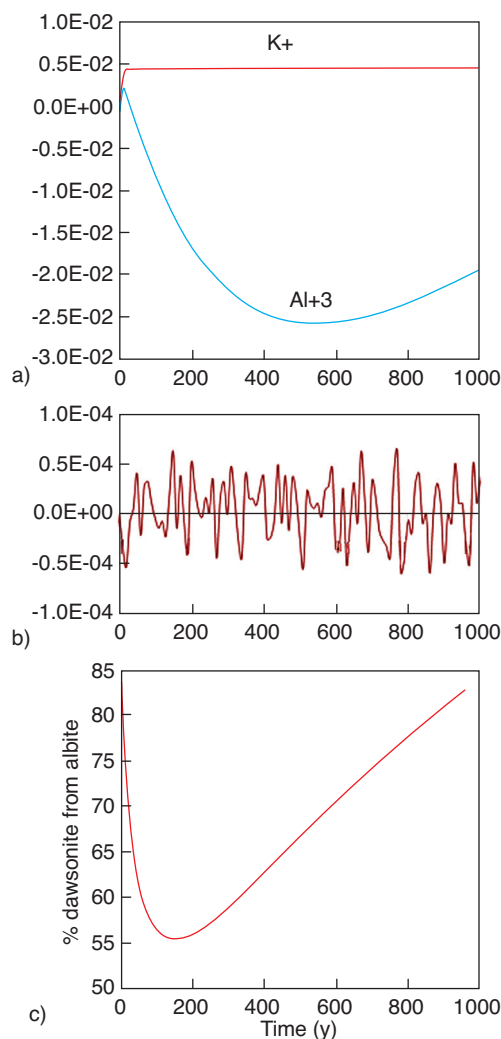

Figure 6

A mass balance in the K-feldspar-kaolinite-muscovite-albite-dawsonite mineral system to estimate the amount of aluminium supplied for dawsonite growth; a) the temporal evolution of aluminium and potassium in the K-feldspar-kaolinite-muscovite (Kkm) mineral assemblage; b) the residual aluminium after withdrawing the excess aluminium in dawsonite compared to albite dissolved, by the amount of aluminium supplied from the Kkm mineral assemblage (6a); and c) the percentage of dawsonite formed from albite.

years and dawsonite is stable and precipitates after 310 years. After reaching dawsonite stability the amount that may potentially form equals (in moles) the amount of albite that dissolves in a system closed to water flow.

The effect of formation water salinity on the temporal evolution of the saturation states of dawsonite is shown in Figure 7. In these simulations dawsonite precipitation is disabled to capture the supersaturations. The waters are assumed to be in equilibrium with calcite and all formation waters immediately reach supersaturation with respect to dawsonite. At seawater NaCl-levels the maximum supersaturation reached after 1 000 years is approximately 3 to 4 times supersaturation ($SI = 0.52$ or $\Omega = 3.31$), increasing steadily following albite dissolution. At 1 and 2 molar NaCl this increases to $SI = 0.76$ and $SI = 1.02$ which correspond to 5.75 and 10.47 times supersaturated solutions respectively after 1 000 years.
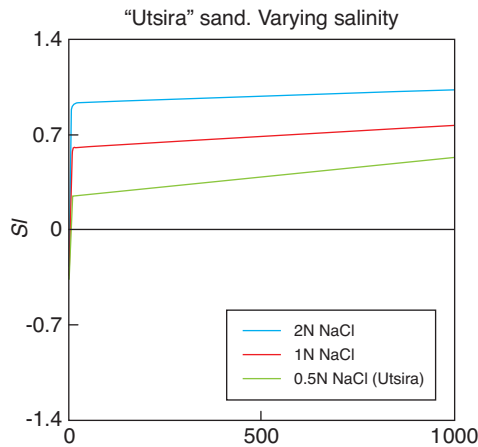
Figure 7

The dawsonite solubility index $SI = \log(q/K)$ for *versus* time for mineralogy, temperature and a CO_2 pressure that correspond to the "Utsira" case, but with varying aqueous NaCl from seawater like 0.5N up to 2N.

2.3 Dawsonite Saturation as a Function of Temperature and Pressure in Quartz-Dominated Reservoirs

Following the simulations on the saturation states and potential of dawsonite formation at Utsira conditions (37°C, 100 bar CO_2), we used the same mineralogy and formation water chemistry and looked at the temporal evolution of saturation states and pH at higher pressures and temperatures. The higher temperatures has a direct effect on all mineral reaction rates through the Arrhenius term in Equations (9) and (13) and the effect on CO_2 solubilities and activity coefficients, whereas higher pressures have indirect effects through increased CO_2 solubilities and lowering of the pH.

Figure 8 shows the evolution of the solubility index of dawsonite and pH with time for 75°C at 200 bar and 120°C at 300 bar compared to the Utsira conditions. The dawsonite precipitation is again disabled to capture the supersaturations. The medium and high temperature cases correspond to CO_2 fugacities of 86.44 and 139.77. The figure shows that the initial saturation states of dawsonite are progressively lower at increasing reservoir depth (increasing temperatures and pressures). The time needed to reach saturation for the given initial formation waters and mineralogy is 170 and 270 years respectively for the 75 and 120°C cases, whereas the "Utsira" case is immediately at saturation. However, as the temperature increases the mineral reactions progress faster. After 500 years the 75°C case has a higher supersaturation than for the base "Utsira" case. The faster reaction rates at elevated temperatures can also be read from the pH as higher temperatures react more minerals faster and buffers the pH to higher values.
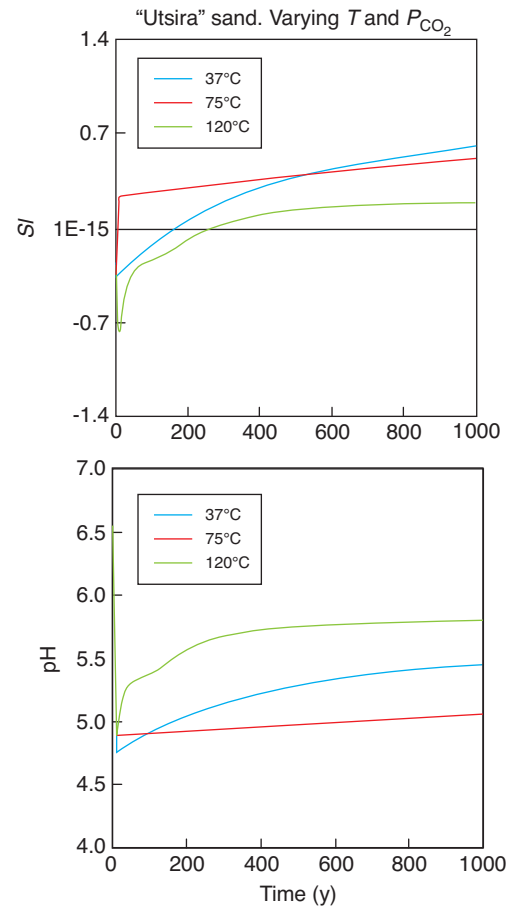

Figure 8

The dawsonite solubility index $SI = \log(q/K)$ and pH *versus* time for the "Utsira" case but with varying temperatures and pressures. Temperatures of 37, 75, and 120°C have corresponding CO_2 pressures of 100, 200 and 300 bar.

Eventually, as suggested by equilibrium thermodynamics *(Fig. 1, 2)*, at amorphous silica or quartz saturation the aluminosilicates are relatively more stable than dawsonite at elevated temperatures and at 120°C dawsonite never reaches more than a minor supersaturation. For all cases the amount of dawsonite that forms approaches the amount (in moles) of albite dissolved if we use the reaction rate law as given by Equations (9) to (11).

As we showed by reactions (1) and (3) and Figure 3 the stability of dawsonite is a function of the CO_2 fugacity with reduced stabilities at lower fugacities. As the CO_2 pressure may show spatial variation in a CO_2 injection system we performed simulations at different CO_2 pressures from 1 to 200 bar at 75°C to see how the pressure variation affects the stability of dawsonite. The mineralogy and initial aqueous solution corresponded to the "Utsira" values listed in Tables 2 and 3, and calcite was chosen as an equilibrium phase.
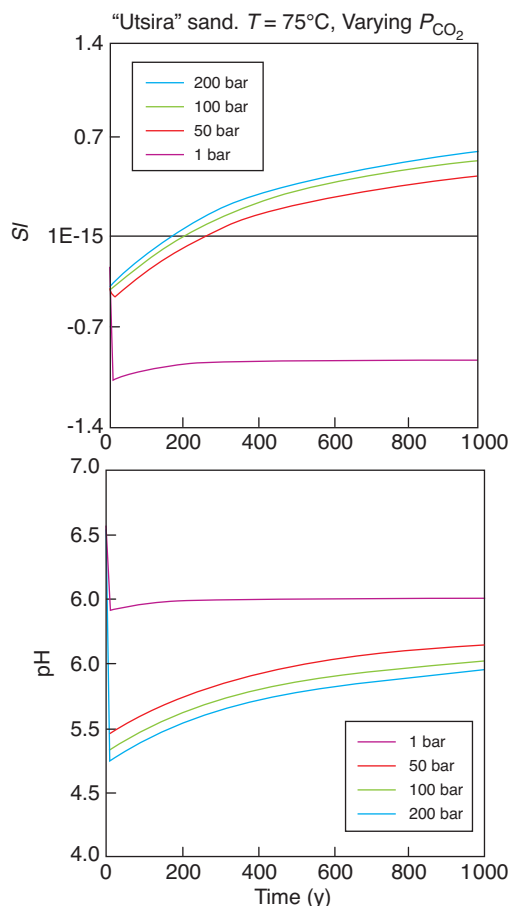
Figure 9

The stability of dawsonite illustrated by the solubility index $SI = \log(q/K)$ and the aqueous pH showed *versus* time for the "Utsira" case mineralogy and initial aqueous solution but at 75°C and with varying CO_2 pressures from 1 to 200 bar.

Figure 9 shows the temporal evolution of the solubility index of dawsonite and pH at the various CO_2 pressures. The simulations suggests that the saturation state of dawsonite and pH is little affected in the range 50 to 200 bar at this temperature. However, the stability limit of dawsonite is reached somewhere between 1 and 50 bar and at 1 bar dawsonite is kept at a *SI* of around -1 for the entire simulated time which correspond to 10 times undersaturation.

2.4 Dawsonite Formation Following CO_2 Injection into a Feldspar Rich Reservoir

We showed in Section 2.2 that the potential amount of dawsonite that forms is related to the amount of albite that dissolves and the NaCl content of the formation water. In this section we simulate a sediment with a lower quartz fraction and with a high feldspar content. The mineral fractions *(Tab. 2)* are modified from the "Gulf-Coast" sediment as

reported by Xu *et al.*, (2007), but with formation waters that corresponds to the base "Utsira" case *(Tab. 3)*. The temperature and CO_2 pressure were set to 75°C and 200 bar respectively. The original mineralogy given in Xu *et al.* (2007) was modified as follows: The Na-rich feldspar, Na-smectite, illite, and chlorite listed in Xu *et al.* (2007) was replaced by albite, Na-montmorillonite, muscovite and clinochlore-14A respectively as these phases were available in the PHREEQC llnl.dat thermodynamic database file. Kinetic parameters were similarly based on the end-member mineral phases rather than for the solid-solutions *(Tab. 1)*.

Figure 10 shows the predicted mineral behavior during the first 1 000 years following CO_2 injection. The simulation suggests large changes. All feldspar, initially constituting 20% of the reservoir sand, dissolved after approximately 600 years. Massive precipitation of Na-montmorillonite and dawsonite followed the albite dissolution. After approximately 200 years the Na-smectite became unstable and supplied Na together with albite for further dawsonite growth. One simulation designed to monitor the solubility index of dawsonite, but not including it as a kinetic phase showed that the dawsonite precipitation was necessary to drive the dissolution of albite to completion (not shown here). Also following the dissolution of the feldspar and the chlorite is massive formation of chalcedony. The changes are in the same order as observed by Xu *et al.* (2007), but larger as they chose a slightly different approach for the reactive surface area.

TABLE 3

Aqueous solution compositions used as initial values for the different simulations. The table is divided into values that correspond to the Utsira aquifer, and with higher salinities by adding NaCl (seawater, 1.0 and 2.0N NaCl)

Aqueous solutes	Concentrations (mol/kgw)		
	"Utsira"[a]	Medium salinity	High salinity
Na[b]	0.4784	1.0	2.0
Cl	0.5213	1.02	2.02
$Fe_{tot,aq}$	3.58×10^{-5}	3.58×10^{-5}	3.58×10^{-5}
$SiO_{2,aq}$	1.664×10^{-4}	1.664×10^{-4}	1.664×10^{-4}
K	0.0053	0.0053	0.0053
Mg	0.01813	0.01813	0.01813
Ca[c]	9.242×10^{-3}	9.242×10^{-3}	9.242×10^{-3}
Al	1.3×10^{-8}	1.3×10^{-8}	1.3×10^{-8}
HCO_3^{-c}	2.192×10^{-2}	2.192×10^{-2}	2.192×10^{-2}
$f_{O_2,g}$	10^{-69}	10^{-69}	10^{-69}
pH[d]	6.5	6.5	6.5

[a] Utsira data from Johnson *et al.* (2004) except for some minor adjustments (see footnotes).

[b] Na^+ adjusted to ensure that the solution is charge neutral.

[c] Equilibrated with aragonite.

[d] pH estimated from an average North Sea CO_2 pressure curve (Smith and Ehrenberg, 1989) and subsequently equilibrated with calcite.
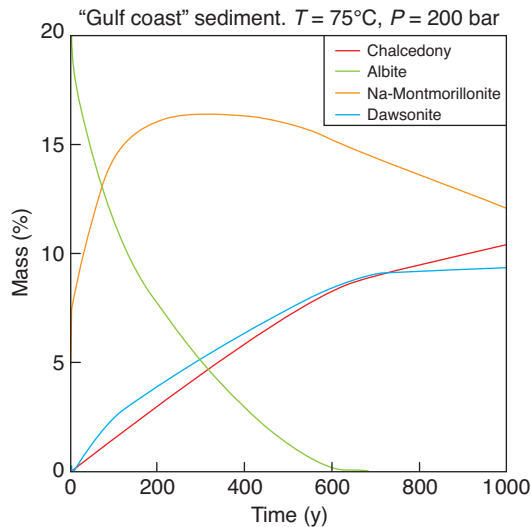
Figure 10

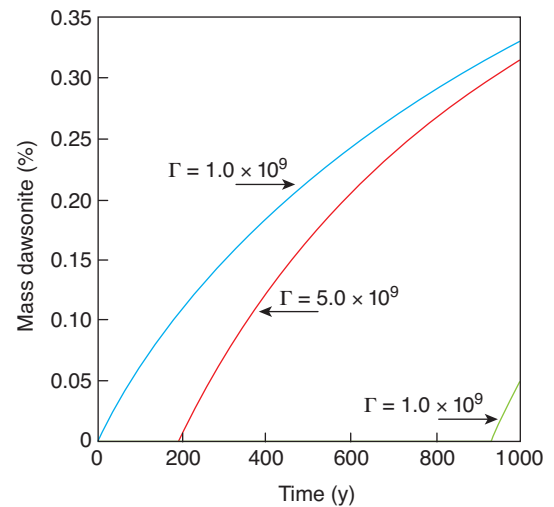Change in mass percent minerals *versus* time for the "Gulf Coast" sediment case at 75°C and 200 bar CO_2.

Figure 11

Mass percent dawsonite for the "Utsira" case varying the nucleation rate parameter Γ from 1×10^9 to 1×10^{10}. At low values, corresponding to fast nucleation at low temperatures, the result is similar to using the TST-derived equation *(Eq. 9) (see Fig. 5)*. At high values, the nucleation rate at low temperature is lower and significant growth is postponed by more than 900 years.

2.5 Dawsonite Formation Using the Modified Rate Law Given by Equation (13)

Equation (13) was constructed to model mineral nucleation and growth and take into account possible differences in rate coefficients and activation energies resulting from differences in reaction mechanisms between under- and oversaturation. The effect on dawsonite growth of varying nucleation rates was examined by varying the nucleation parameter Γ from 10^9 to 10^{10} *(Fig. 11)*. All growth parameters was identical to the Utsira simulation in Section 2.2 where the TST-derived equation was used, except for the initial growth surface area that was calculated by Equation (11) *i.e.* zero initial growth surface area for dawsonite. The mineralogy and the initial formation water corresponded to the "Utsira" case *(Tab. 2, 3)*. The simulations shows that by using a low value of gamma ($\Gamma = 10^9$), which gives high nucleation rates at low temperatures and low supersaturations, dawsonite growth is initiated immediately and the amount that forms over 1 000 years is similar to Section 2.2 simulations shown in Figure 5. This is because the growth in both cases are constrained by the supply rate of aluminium from the dissolving aluminosilicates. At higher values of Γ, 5×10^9 and 10^{10}, giving lower nucleation rates at low supersaturations and low temperatures, significant growth is postponed to approximately 200 and 930 years respectively. The effect of reducing the BCF growth rate coefficient (k_p in *Eq. 13*) relative to the TST-rate coefficient used in Section 2.2 (k_d) was examined using a fixed $\Gamma = 5 \times 10^9$ *(Fig. 12)*. This figure shows the mass percentage of dawsonite formed and the solubility index over 1 000 years. When k_p equals k_d,

an initial period of nucleation at increasing supersaturations is followed by rapid growth after approximately 200 years at close to dawsonite equilibrium. Reducing the precipitation rate coefficient leads to a longer time before the growth part of Equation (13) dominates, followed by growth at slightly oversaturated solutions. The difference in the amount of dawsonite that formed at the end of the simulations is however small compared to the 5 orders of magnitude difference in growth rate coefficients. This again follows from the fast reaction rates of dawsonite relative to the aluminosilicates supplying aluminium.

3 DISCUSSION

A large number of numerical simulations of CO₂ storage in saline aquifers suggest that dawsonite should form at a great variety of conditions (Cantucci *et al.*, 2009; Johnson *et al.*, 2005; Knauss *et al.*, 2005; White *et al.*, 2005; Xu *et al.*, 2007; Zerai *et al.*, 2006; Zhang *et al.*, 2009). Common for these simulations is the use of a simplified version of the general TST-derived rate law for mineral reactions (see Lasaga, 1984; Aagaard and Helgeson, 1982). Solving this rate equation results in precipitation of minerals without taking into account an initial nucleation phase preceding growth. Moreover, the TST-derived rate laws are only valid if the same mechanism is responsible for both the dissolution and precipitation (see Lasaga, 1984; Aagaard and Helgeson,
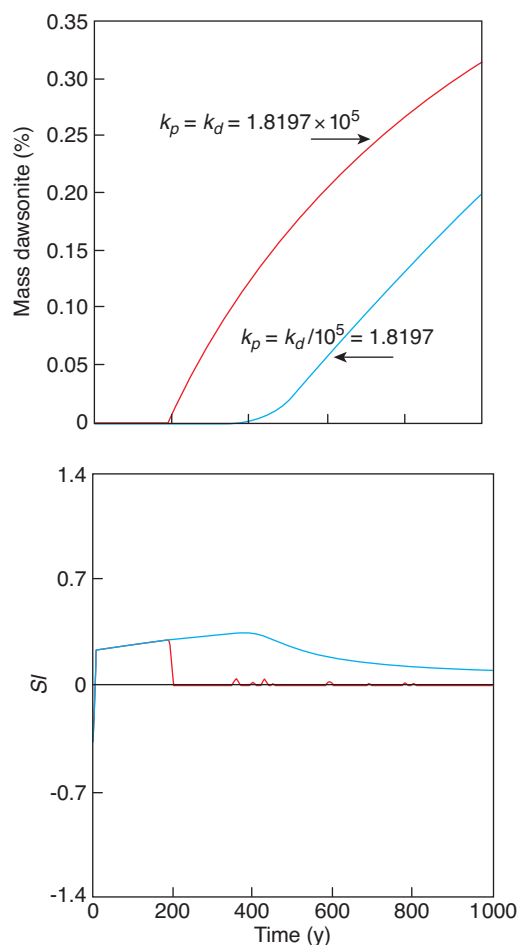
Figure 12

The mass percent dawsonite and the saturation index *SI* for dawsonite for the "Utsira" case at varying precipitation rate coefficients k_p, and fixed $\Gamma = 5 \times 10^9$ and $k_N = 1 \times 10^{-8}$. The simulations suggest that reducing the dawsonite precipitation rate coefficient by 5 orders of magnitude postpone significant precipitation by 200 years, whereas the amount that forms after 1 000 years is only 37% lower.

1982). There is at present no direct experimental data available giving dawsonite reaction rates and mechanisms as a function of affinity. The far-from-equilibrium dissolution rate experiments by Hellevang *et al.* (2010) shows that dawsonite dissolution is rapid down to room temperatures. The equally far-from-equilibrium oversaturated growth experiments by Duan *et al.* (2005) shows dawsonite growth down to 75ºC, with rates probably limited by the dissolution rates of the aluminium source (see introduction this report).

In the present study we suggest a new rate equation *(Eq. 13)* that separates dissolution and growth and that includes an upscaled nucleation term derived from classical nucleation theory. The dissolution part is the TST-derived expression commonly used to model mineral reactions, whereas the growth part correspond to BCF growth, which appears to explain precipitation rates of minerals like magnesite (Saldi *et al.*, 2009), calcite (Shiraki and Brantley, 1995), dolomite (Arvidson and Mackenzie, 1997, 1999) and quartz (Ganor *et al.*, 2005). Because no information is available for the reaction rates of dawsonite close to saturation, we varied parameters like the precipitation rate coefficient and the nucleation parameter Γ *(Eq. 13)* to learn about the sensitivity of dawsonite growth on these parameters. Moreover, we disabled dawsonite growth and varied parameters like temperature, salinity, and CO_2 pressure to see how high oversaturations dawsonite reached.

From our sensitivity study on mineralogy, temperature and pressure we conclude that dawsonite is unlikely to reach very high supersaturations. For Utsira conditions (37°C, 100 bar CO_2) and seawater-type aqueous solution equilibrated with calcite the maximum saturation at 1 000 years was 3-4 times oversaturated *(Fig. 8)*. Within the range of parameters used for nucleation in the present study ($10^9 < \Gamma < 10^{10}$; $k_N = 10^{-8}$ moles/s) these oversaturations were sufficient to produce dawsonite *(Fig. 11, 12)*. However, as no information is available on the size of these parameters, the simulations can only be used as an indication of the sensitivity of dawsonite growth and cannot exclude that it is a low-temperature nucleation barrier that prevents dawsonite formation. At medium temperature (75-100ºC) the thermodynamic stability diagrams shows that dawsonite is thermodynamic stable at quartz saturation *(Fig. 1-3)*, and with exponential increasing nucleation and growth rates these conditions seems to be favorable for dawsonite formation. At high temperatures, the thermodynamic stability of dawsonite relative to the aluminosilicates diminishes again reducing the possibility for dawsonite growth *(Fig. 2)*.

The present simulations on the sensitivity of dawsonite growth on rate and nucleation parameters are valuable to distinguish important from less important factors. We showed that changing the precipitation rate coefficient by 5 orders of magnitude had little effect on the amount of dawsonite that formed, whereas the onset of growth dominated by the BCF part of Equation (13) was seen highly sensitive to the nucleation parameters. However, to fully understand the potential of dawsonite growth and more generally the potential of carbonate formation in low-temperature reservoirs like the Utsira Sand more experimental work on nucleation and growth rates at various temperatures and affinities are clearly needed.

SUMMARY AND CONCLUSIONS

Dawsonite is observed to form in natural reservoirs at high CO_2 pressures typically replacing Na-feldspars, and as a pore-filling cement The observations are however few in quartz-rich shallow "cold" reservoirs such as the North Sea

Utsira Sand that is at present used as a storage host for CO_2. Numerical simulations of CO_2 storage on the other hand predict dawsonite formation as a dominant mineral carbonate for most reservoir types and down to low temperatures (*e.g.*, Johnson *et al.*, 2004; Knauss *et al.*, 2005; Xu *et al.*, 2004, 2007; Zerai *et al.*, 2006). Common for all these simulations are the use of a TST-derived kinetic expression that consists of one term taking into account the effect of affinity for both dissolution and precipitation. We suggest a new rate equation *(Eq. 13)* that separates dissolution and growth and that includes an upscaled nucleation term derived from classical nucleation theory. The dissolution part is the TST-derived expression commonly used to model mineral reactions, whereas the growth part correspond to BCF growth, which appears to explain precipitation rates of minerals like magnesite (Saldi *et al.*, 2009), calcite (Shiraki and Brantley, 1995), dolomite (Arvidson and Mackenzie, 1997, 1999) and quartz (Ganor *et al.*, 2005).

As expected, the simulations suggest that the maximum potential of dawsonite growth is tightly linked to the temperature of the reservoir and the amount of reacting phases that provide aluminium and sodium. Moreover, we showed that changing the precipitation rate coefficient of dawsonite by 5 orders of magnitude had little effect on the amount of dawsonite that formed, whereas the onset of growth dominated by the BCF part of Equation (13) was seen highly sensitive to the nucleation parameters. Finally, based on thermodynamic considerations, numerical simulations and comparisons to precipitation rates of related carbonates we suggest that the potential of dawsonite growth is limited to a window framed by a high thermodynamic stability relative to competing mineral phases at low temperatures, but with rapidly diminishing precipitation rates at lower temperatures constrained by an activation energy barrier. As experiments on the dawsonite growth rate has not yet been reported, except for the limited data given by Duan *et al.* (2005), the sensitivity study presented in this work can only be though of as an indication of the potential of dawsonite growth based on related minerals. Thus, to finally understand the potential of dawsonite growth at reservoir conditions it is clearly a need for more experimental work on dawsonite precipitation rates, most importantly as a function of temperature and affinity.

ACKNOWLEDGMENTS

REFERENCES

Aagaard P., Helgeson H.C. (1982) Thermodynamic and kinetic constraints on reaction rates among minerals and aqueous solutions I. Theoretical considerations, *Am. J. Sci.* **282**, 237-285.

Aagaard P., Egeberg P.K., Saigal G.C., Morad S., Bjørlykke K. (1990) Diagenetic albitization of detrital K-feldspar in Jurassic, Lower Cretaceous, and Tertiary clastic reservoir rocks from offshore Norway, II. Formation water chemistry and kinetic considerations, *J. Sediment. Petrol.* **60**, 575-581.

Aagaard P., Pham V.T.H., Hellevang H. (2009) A modeling study of the log-term mineral trapping in deep saline marine sand aquifers, *American Geophysical Union, Fall Meeting*, San Francisco, CA, USA. abstract #H12B-07.

Aja S.U., Rosenberg P.E., Kittrick J.A. (1991) Illite equilibria in solutions: I. Phase relationships in the system $K_2O-Al_2O_3-SiO_2-H_2O$ between 25 and 250ºC, *Geochim. Cosmochim. Ac.* **55**, 1353-1364.

André L., Audigane P., Azaroual M., Menjoz A. (2007) Numerical modeling of fluid-rock chemical interactions at the supercritical CO_2-liquid interface during CO_2 injection into a carbonate reservoir, the Dogger aquifer (Paris Basin, France), *Energ. Convers. Manage.* **48**, 6, 1782-1797.

Arvidson R.S., Mackenzie F.T. (1997) Tentative kinetic model for dolomite precipitation rate and its application to dolomite distribution, *Aquat. Geochem.* **2**, 273-298.

Arvidson R.S., Mackenzie F.T. (1999) The dolomite problem: control of precipitation kinetics by temperature and saturation state, *Am. J. Sci.* **299**, 257-288.

Baker J.C., Bai G.P., Hamilton P.J., Golding S.D., Keene J.B. (1995) Continental-scale magmatic carbon dioxide seepage recorded by dawsonite in the Bowen-Gunnedah-Sydney Basin system, Eastern Australia, *J. Sediment. Res.* **A65**, 3, 522-530.

Bauer A., Berger G. (1998) Kaolinite and smectite dissolution rate at high molar KOH solutions at 35 and 80ºC, *Appl. Geochem.* **13**, 7, 905-916.

Bénézeth P., Palmer D.A., Anovitz L.M., Horita J. (2007) Dawsonite synthesis and reevaluation of its thermodynamic properties from solubility measurements: Implications for mineral trapping of CO_2, *Geochim. Cosmochim. Ac.* **71**, 18, 4438-4455.

Bjørlykke K., Nedkvitne T., Ramm M., Saigal G.C. (1992) Diagenetic processes in the Brent Group (Middle Jurassic) reservoirs of the North Sea: an overview, *Geol. Soc. London Spec. Pub.* **61**, 263-287.

Bjørlykke K., Egeberg P.K. (1993) Quartz cementation in sedimentary basins, *Am. Association Petroleum Geologists Bull.* **77**, 9, 1538-1548.

Blum A.E. Stillings L.L. (1995) Feldspar dissolution kinetics, *Rev. Mineral. Geochem.* **31**, 1, 291-351.

Brandt F., Bosbach D., Krawczyk-Bärsch E., Arnold T., Bernhard G. (2003) Chlorite dissolution in the acid ph-range: a combined microscopic and macroscopic approach, *Geochim. Cosmochim. Ac.* **67**, 8, 1451-1461.

Brantley S.L. (2008) Kinetics of mineral dissolution, in *Kinetics of water-rock interaction*, Brantley S.L., Kubicki J.D., White A.F. (eds), Springer Science + business Media, LLC, New York, pp. 151-196.

Brunauer S., Emmett P.H., Teller E. (1938) Adsorption of gases in multimolecular layers, *J. Am. Chem. Soc.* **60**, 309-319.

Burton W.K., Cabrera N., Frank F.K. (1951) The growth of crystals and the equilibrium structure of their surfaces, *Philos. T. Roy. Soc. London* **243**, 299-358.

Cantucci B., Montegrossi G., Vaselli O., Tassi F., Quattrocchi F., Perkins E.H. (2009) Geochemical modeling of CO_2 storage in deep reservoirs: The Weyburn Project (Canada) case study, *Chem. Geol.* **265**, 1-2. 181-197.

Carroll-Webb S.A., Walther J.V. (1988) A surface complex reaction model for the pH-dependence of corundum and kaolinite dissolution rates, *Geochim. Cosmochim. Ac.* **52**, 11, 2609-2623.

Chadwick R.A., Zweigel P., Gregersen U., Kirby G.A., Holloway S., Johannessen P.N., (2004) Geological reservoir characterization of a CO_2 storage site: The Utsira Sand, Sleipner, northern North Sea, *Energy* **29**, 9-10, 1371-1381.

Duan R., Carey J.W., Kaszuba J.P. (2005) Mineral chemistry and precipitation kinetics of dawsonite in the geological sequestration of CO_2, *American Geophysical Union, Fall Meeting 2005*, abstract #GC13A-1210.

Ehrenberg S.N., Nadeau P.H. (1989) Formation of diagenetic illite in sandstones of the Garn Formation, Haltenbanken area, Mid-Norwegian Continental shelf, *Clay Miner.* **24**, 233-253.

Eslinger E., Pevear D. (1988) *Clay minerals for petroleum geologists and engineers*, Society of Economic Palaeontologists and Mineralogists; Short Course Notes, 22.

Ferrante M.J., Stuve J.M., Richardson D.W. (1976) *Thermodynamic data for synthetic dawsonite. Report of investigations* - U.S. Bureau of Mines, 8129, 13 p.

Gale J. (2004) Geological storage of CO_2: What do we know, where are the gaps and what more needs to be done? *Energy* **29**, 1329-1338.

Ganor J., Huston T.J., Walter L.M. (2005) Quartz precipitation kinetics at 180ºC in NaCl solutions - Implications for the usability of the principle of detailed balancing, *Geochim. Cosmochim. Ac.* **69**, 8, 2043-2056.

Gao Y., Liu L., Hu W. (2009) Petrology and isotopic geochemistry of dawsonite-bearing sandstones in Hailaer basin, northeastern China, *Appl. Geochem.* **24**, 9, 1724-1738.

Gaus I., Le Guern C., Pauwels H., Girard J.-P., Pearce J., Shepherd T., Hatziyannis G., Metaxas A. (2004) Comparison of long term geochemical interactions at two natural CO_2-analogues: Montmiral (Southeast Basin, France) and Messokampos (Florina Basin, Greece) case studies, *GHGT7-7th International Conference on Greenhouse Gas Control Technologies*, Vancouver, Canada, 5-9 September 2004, 9 p.

Gaus I., Azaroual M., Czernichowski-Lauriol I. (2005) Reactive transport modelling of the impact of CO_2 injection on the clayey cap rock at Sleipner (North Sea), *Chem. Geol.* **217**, 3-4, 319-337.

Gherardi F., Xu T., Pruess K. (2007) Numerical modeling of self-limiting and self-enhancing caprock alteration induced by CO_2 storage in a depleted gas reservoir, *Chem. Geol.* **244**, 1-2, 103-129.

Giammar D.E., Bruant Jr R.G., Peters C.A. (2005) Forsterite dissolution and magnesite precipitation at conditions relevant for deep saline aquifer storage and sequestration of carbon dioxide, *Chem. Geol.* **217**, 257-276.

Golab A.N., Carr P.F., Palamara D.R. (2006) Influence of localised igneous activity on cleat dawsonite formation in Late Permian coal measures, Upper Hunter Valley, Australia, *Int. J. Coal Geol.* **66**, 296-304.

Golab A.N., Hutton A.C., French D. (2007) Petrography, carbonate mineralogy and geochemistry of thermally altered coal in Permian coal measures, Hunter Valley, Australia, *Int. J. Coal Geol.* **70**, 1-3, 150-165.

Golubev S.V., Bauer A., Pokrovsky O.S. (2006) Effect of pH and organic ligands on the kinetics of smectite dissolution at 25°C, *Geochim. Cosmochim. Ac.* **70**, 17, 4436-4451.

Harrison W.J., Wendlandt R.F., Dendy Sloan E. (1995) Geochemical interactions resulting from carbon dioxide disposal on the seafloor, *Appl. Geochem.* **10**, 4, 461-475.

Hellevang H., Declercq J., Kvamme B., Aagaard P. (2010) The dissolution rates of dawsonite at pH 0.9 to 6.3 and temperatures of 22, 60 and 77ºC, *Appl. Geochem.* **25**, 1575-1586.

Hellevang H., Aagaard P., Oelkers E.H., Kvamme B. (2005) Can dawsonite permanently trap CO_2? *Environ. Sci. Technol.* **39**, 21, 8281-8287.

Holloway S. (1997) An overview of the underground disposal of carbon dioxide, *Energ. Convers. Manage.* **38**, 193-198.

IPCC (2005) Chapter 5 Underground geological storage, in *Carbon dioxide capture and storage*, Metz B., Davidson O., de Coninck H., Loos M., Meyer L. (eds), Cambridge University Press, Cambridge, UK, pp. 431.

IPCC (2007) *WG II: Impacts, adaption and vulnerability*, Parry M.L., Canziani O.F., Palutikof J.P., van der Linden P.J., Hanson C.E. (eds), Cambridge University Press, Cambridge, UK, pp. 976.

Johnson J.W., Nitao J.J., Knauss K.G. (2004) Reactive transport modeling of CO_2 storage in saline aquifers to elucidate fundamental processes, trapping mechanisms and sequestration partitioning, in *Geological storage of carbon dioxide*, Bains S.J., Worden R.H. (eds), Geological Society Special Publications, London, pp. 107-128.

Johnson J.W., Nitao J.J., Morris J.P. (2005) *Reactive Transport Modeling of Cap-Rock Integrity During Natural and Engineered CO_2 Storage, Carbon Dioxide Capture for Storage in Deep Geologic Formations*, Elsevier Science, Amsterdam, pp. 787-813.

Johnson J.W., Oelkers E.H., Helgeson H.C. (1992) SUPCRT92: A software package for calculating the standard molal thermodynamic properties of minerals, gases, aqueous species, and reactions from 1 to 5 000 bar and 0 to 1 000°C, *Comput. Geosci.* **18**, 7, 899-947.

Ketzer J.M., Iglesias R., Einloft S., Dullius J., Ligabue R., de Lima V. (2009) Water-rock-CO_2 interactions in saline aquifers aimed for carbon dioxide storage: Experimental and numerical modeling studies of the Rio Bonito Formation (Permian), southern Brazil, *Appl. Geochem.* **24**, 5, 760-767.

Knauss K.G., Johnson J.W., Steefel C.I. (2005) Evaluation of the impact of CO_2, co-contaminant gas, aqueous fluid and reservoir rock interactions on the geologic sequestration of CO_2, *Chem. Geol.* **217**, 3-4, 339-350.

Lasaga A.C. (1981) Transition state theory, in *Kinetics of Geochemical Processes*, Lasaga A.C., Kirkpatrick R.J. (eds), Mineralogical Society of America, pp. 135-169.

Lasaga A.C. (1984) Chemical kinetics of water-rock interactions, *J. Geophys. Res.* **89**, 4009-4025.

Moore J., Adams M., Allis R., Lutz S., Rauzi S. (2005) Mineralogical and geochemical consequences of the long-term presence of CO_2 in natural reservoirs: An example from the Springerville-St. Johns Field, Arizona, and New Mexico, U.S.A., *Chem. Geol.* **217**, 3-4, 365-385.

Nagy K.L., Lasaga A.C. (1992) Dissolution and precipitation kinetics of gibbsite at 80ºC and pH 3: The dependence on solution saturation state, *Geochim. Cosmochim. Ac.* **56**, 3093-3111.

Nielsen A.E. (1964) *Kinetics of precipitation*, Pergamon Press, Oxford.

Nordstrom D.K., Plummer L.N., Wigley T.M.L., Wolery T.J., Ball J.W., Jenne E.A., Bassett R.L., Crerar D.A., Florence T.M., Fritz B., Hoffman M., Holdren Jr G.R., Lafon G.M., Mattigod S.V., McDuff R.E., Morel F., Reddy M.M., Sposito G., Thrailkill J. (1979) A comparison of computerized chemical models for equilibrium calculations in aqueous systems, in *Chemical modeling in aqueous systems, speciation, sorption, solubility, and kinetics*, Jenna E.A. (ed.), American Chemical Society, pp. 857-892.

Oelkers E.H., Schott J., Gauthier J.-M., Herrero-Roncal T. (2008) An experimental study of the dissolution mechanism and rates of muscovite, *Geochim. Cosmochim. Ac.* **72**, 20, 4948-4961.

Pauwels H., Gaus I., le Nindre Y.M., Pearce J., Czernichowski-Lauriol I. (2007) Chemistry of fluids from a natural analogue for a geological CO_2 storage site (Montmiral, France): Lessons for CO_2-water-rock interaction assessment and monitoring, *Appl. Geochem.* **22**, 2817-2833.

Parkhurst D.L., Appelo C.A.J. (1999) User's guide to PHREEQC (version 2) - a computer program for speciation, reaction-path, 1D-transport, and inverse geochemical calculations, *US Geological Survey, Water Resources Investigation Reports*, pp. 312.

Pearce J.M., Holloway S., Wacker H., Nelis M.K., Rochelle C., Bateman K. (1996) Natural occurrences as analogues for the geological disposal of carbon dioxide, *Energ. Convers. Manage.* **37**, 6-8, 1123-1128.

Pokrovsky O.S., Golubev S.V., Schott J., Castillo A. (2009) Calcite, dolomite and magnesite dissolution kinetics in aqueous solutions at acid to circumneutral pH, 25 to 150°C and 1 to 55 atm pCO_2: New constraints on CO_2 sequestration in sedimentary basins, *Chem. Geol.* **265**, 1-2, 20-32.

Saigal G.C., Morad S., Bjørlykke K., Egeberg P.K., Aagaard P. (1988) Diagenetic albitization of detrital K-feldspar in Jurassic, Lower Cretaceous, and Tertiary clastic reservoir rocks from offshore Norway, I. Texture and origin, *J. Sediment. Petrol.* **58**, 1003-1013.

Saldi G.D., Jordan G., Schott J., Oelkers E.H. (2009) Magnesite growth rates as a function of temperature and saturation state, *Geochim. Cosmochim. Ac.* **73**, 19, 5646-5657.

Shiraki R., Brantley S.L. (1995) Kinetics of near-equilibrium calcite precipitation at 100°C: An evaluation of elementary reaction-based and affinity-based rate laws, *Geochim. Cosmochim. Ac.* **59**, 8, 1457-1471.

Smith J.W., Milton C. (1966) Dawsonite in the Green River Formation of Colorado, *Econ. Geol.* **61**, 1029-1042.

Soave G. (1972) Equilibrium constants from a modified Redlich-Kwong equation of state, *Chem. Eng. Sci.* **27**, 1197-1203.

Tester J.W., Worley W.G., Robinson B.A., Grigsby C.O., Feerer J.L. (1994) Correlating quartz dissolution kinetics in pure water from 25 to 625°C, *Geochim. Cosmochim. Ac.* **58**, 11, 2407-2420.

Walton A.G. (1963) Nucleation and the interfacial tension of sparingly soluble salts, *Microchim. Acta* **51**, 3, 422-430.

Walton A.G. (1967) *The formation and properties of precipitates*, Interscience Publishers, New York, pp. 232.

White S.P., Allis R.G., Moore J., Chidsey T., Morgan C., Gwynn W., Adams M. (2005) Simulation of reactive transport of injected CO_2 on the Colorado Plateau, Utah, USA, *Chem. Geol.* **217**, 3-4, 387-405.

Wigand M., Carey J.W., Schütt H., Spangenberg E., Erzinger J. (2008) Geochemical effects of CO_2 sequestration in sandstones under simulated in situ conditions of deep saline aquifers, *Appl. Geochem.* **23**, 9, 2735-2745.

Worden R.H. (2006) Dawsonite cement in the Triassic Lam Formation, Shabwa Basin, Yemen: A natural analogue for a potential mineral product of subsurface CO_2 storage for greenhouse gas reduction, *Mar. Petrol. Geol.* **23**, 1, 61-77.

Xu T., Apps J.A., Pruess K. (2004) Numerical simulation of CO_2 disposal by mineral trapping in deep aquifers, *Appl. Geochem.* **19**, 6, 917-936.

Xu T., Apps J.A., Pruess K., Yamamoto H. (2007) Numerical modeling of injection and mineral trapping of CO_2 with H_2S and SO_2 in a sandstone formation, *Chem. Geol.* **242**, 3-4, 319-346.

Zerai B., Saylor B.Z., Matisoff G. (2006) Computer simulation of CO_2 trapped through mineral precipitation in the Rose Run Sandstone, Ohio, *Appl. Geochem.* **21**, 2, 223-240.

Zhang X., Wen Z., Gu Z., Xu X., lin Z. (2004) Hydrothermal synthesis and thermodynamic analysis of dawsonite-type compounds, *J. Solid State Chem.* **177**, 3, 849-855.

Zhang W., li Y., Xu T., Cheng H., Zheng Y., Xiong P. (2009) Long-term variations of CO_2 trapped in different mechanisms in deep saline formations: A case study of the Songliao Basin, China, *Int. J. Greenhouse Gas Control* **3**, 2, 161-180.